THE JOURNAL OF PHYSICAL CHEMISTRY B

ARTICLE

pubs.acs.org/JPCB

Rotational Dynamics of Coumarin-153 and 4-Aminophthalimide in 1-Ethyl-3-methylimidazolium Alkylsulfate Ionic Liquids: Effect of Alkyl Chain Length on the Rotational Dynamics

Sudhir Kumar Das and Moloy Sarkar*

School of Chemical Sciences, National Institute of Science Education and Research, Bhubaneswar 751005, India

ABSTRACT: Rotational dynamics of two neutral organic solutes, coumarin-153 (C-153) and 4-aminophthalimide (AP), with only the latter having hydrogen-bond-donating ability, has been investigated in a series of 1-ethyl-3-methylimidazolium alkyl sulfate ionic liquids as a function of temperature. The ionic liquids differ only in the length of the linear alkyl side chain (alkyl = ethyl, butyl, hexyl, and octyl) on the anionic moiety. The present study has been undertaken to examine the role of alkyl side chains on the rotational dynamics of the two solutes in these ionic liquids. Analysis of the results using Stokes−Einstein−Debye hydrodynamic theory indicates that the rotational dynamics of C-153 lies between the stick and slip boundary condition in the ethyl analogue and finally reaches subslip condition as in case of the octyl substituent. The observed rotational behavior of C-153 has been explained on the basis of an increase in the size of the solvent, which offers lower friction for solute rotation. On the other hand, AP shows superstick behavior in the ethyl system and exceeds the stick limit in the octyl derivative. Superstick behavior of AP has been attributed to the specific hydrogen-bonding interaction between AP and the sulfate moiety. Proton NMR investigation confirms the hydrogen-bonding interaction between the N−H hydrogen of AP and the ionic liquid. The decrease in rotational coupling constant values for AP with increasing length of alkyl side chains has been attributed to the decrease in the solute−solvent-specific interaction with an increase in the alkyl side chain length on the sulfate moiety.

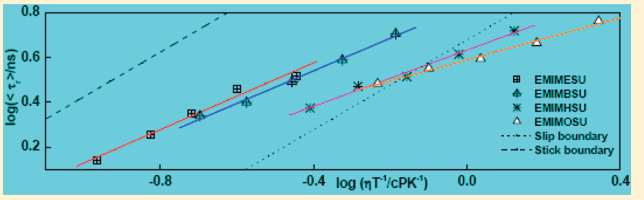

INTRODUCTION

In recent times, room-temperature ionic liquids (RTILs) have drawn considerable attention due to their wide range of applications toward chemical, material, and biological sciences.[1−12] The emergence of the RTILs as specialty media or materials has been possible by virtue of their interesting physicochemical properties, such as wide liquids range, negligible vapor pressure, and high viscosity. Ionic liquids are also known to be microheterogeneous in nature.[13,14] Interionic interactions in these RTILs are believed to be an important factor for their interesting properties.[6,11] Since the interplay between intermolecular forces may give rise to nontrivial behavior of the ionic liquids, closer investigation of the intermolecular interactions is required to have a thorough knowledge of their physicochemical properties. Dielectric relaxation,[15,16] solvation dynamics,[17−27] rotational diffusion,[20−35] and intramolecular electron/charge transfer[36−38] are some of the studies which have been carried out in recent times to address these issues. It may be mentioned that studies on orientational dynamics are often helpful to find out specific solute−solvent interactions.[39] Even though available literature on the rotational dynamics of various solutes in conventional solvents is quite extensive, similar information on ionic liquids is rather limited.

Ingram et al.[21] studied the rotational dynamics of *N*,*N*′-bis(2,5-di-*tert*-butylphenyl)-3,4,9,10-perylenecarboximide (BTBP) and 4-aminophthalimide (AP) in 1-butyl-3-methylimidazolium hexafluorophasphate, [BMIM][PF_6], as a function of temperature. Ito et al.[22,23] also studied the rotational dynamics of neutral and charged solutes in the same ionic liquid. These studies revealed that the rotational dynamics of the organic solutes are mainly governed by the viscosity of the medium. However, no evidence of the electrostatic and/or specific hydrogen-bonding interactions has been found.

Interestingly, Mali et al.[29,30] have shown that solute−solvent (IL) hydrogen-bonding interaction in the RTILs significantly hinders solute rotation. The effect of specific solute−solvent hydrogen-bonding interaction on the rotational dynamics of a neutral organic solute has also been observed by Paul et al.[20] in an alcohol-functionalized IL. In recent times, rotational dynamics of ionic solutes have also been carried out in different ionic liquids to throw more light on solute−solvent interaction.[31−35] Fruchey and Fayer[34] studied the rotational diffusion of a charged solute, sodium 8-methoxypyrene-1,3,6-sulfonate (MPTS), and a neutral solute, perylene, in a series of 1-alkyl-3-methylimidazolium bis-(trifluoromethanesulfonyl)imide RTILs. Anionic MPTS is found to exhibit superstick behavior due to its strong interaction with the imidazolium cation of the ILs. However, the rotational motion of perylene becomes increasingly subslip with increasing alkyl chain length of the cationic moiety. A similar rotational dynamics study of ionic solutes in 1-butyl-3-methylimidazolium tetrafluoroborate, [bmim][BF_4], and glycerol by Samanta and co-workers[35] reveals that there is no observable effect of electrostatic interaction between these ionic solutes and the ionic liquid.

Received: August 5, 2011
Revised: November 21, 2011
Published: November 23, 2011

Chart 1. Structure of (A) Coumarin-153, (B) 4-Aminophthalimide, and (c) RTILs

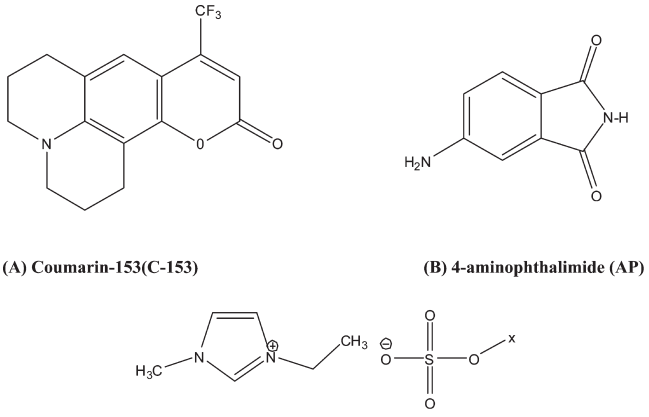

(A) Coumarin-153(C-153) (B) 4-aminophthalimide (AP)

(C) 1-ethyl-3-methylimidazolium alkylsulfate (x= C_2H_5, C_4H_9, C_6H_{13} and C_8H_{17})

However, a hydrogen-bonding interaction is found to play an important role toward the rotational motion of the solutes. Dutt and co-workers[31] also studied the rotational behavior of rhodamine 110 (R110) and 2,5-dimethyl-1,4-dioxo-3,6-diphenylpyrrolo[3,4-*c*]pyrrole (DMDPP) in a series of 1-alkyl-3-methylimidazolium ionic liquids containing fluoroalkylphosphate (FAP) anions. They observed that the rotational behavior of R110 is closer to the stick boundary condition due to the specific solute−solvent interaction, whereas DMDPP follows slip hydrodynamics. Interestingly, the rotational behavior of DMDPP is found not to be influenced by the alkyl chain lengths.

It is therefore evident from the above discussions that the exact nature of solute−solvent interactions in the ILs is still not clear. Study of the rotational dynamics by doing the systematic variations in the constituents of the ILs would be helpful to understand the nature of various forces that are responsible for solute−solvent interactions and also the interactions between the constituents of the ILs. While the effect of alkyl chain length on the cationic part of the ILs toward the rotational dynamics of organic solutes in the ILs has been demonstrated by Fayer[34] and Dutt[31] independently, no studies on this aspect by varying the alkyl chain length in the anionic part of the ILs have been carried out.

Keeping this in mind, we have undertaken the present study in which the dynamics of rotational diffusion of two neutral organic solutes, 4-aminophthalimide (AP) and coumarin 153 (C-153), have been investigated in a series of 1-ethyl-3-methylimidazolium alkyl sulfate ionic liquids, viz. 1-ethyl-3-methylimidazolium ethylsulfate (EMIMESU), 1-ethyl-3-methylimidazolium butylsulfate (EMIMBSU), 1-ethyl-3-methylimidazolium hexylsulfate (EMIMHSU), and 1-ethyl-3-methyl imidazolium octylsulfate (EMIMOSU), as a function of temperature. These ILs are purposefully chosen to maintain a systematic variation of the alkyl group in their anionic moiety. Both probes are suitable for rotational dynamics study in organic medium.[20,40,41] Out of the probes, only AP has the hydrogen-bond-donating ability by virtue of its polarized N−H fragment.[42] Sulfate-containing ionic liquids are chosen so that they can form a hydrogen bond with AP. Structural information of the solutes and ionic liquids is provided in Chart 1.

MATERIALS AND EXPERIMENTAL TECHNIQUES

AP is obtained from TCI (Japan) and recrystallized from ethanol .The purity of the compound is confirmed by the spectral measurements. C-153 (laser grade, Excitation) is used as received. The ionic liquids are obtained from Merck Germany (>99% purity) with <100 ppm water content and halide concentration. Proper precaution is taken to avoid moisture absorption by the media during the measurements.

The viscosities (η) of the RTIL are measured by a LVDV-III Ultra Brookfield Cone and Plate viscometer (1% accuracy and 0.2% repeatability). An Anton Paar (DMA 5000) density meter is used to measure the densities of the ILs. Time-resolved anisotropy decay measurements were carried out using a time-correlated single-photon counting (TCSPC) spectrometer (Edinburgh, OB920). A diode laser (375 nm) was used as the excitation source, and a MCP photomultiplier (Hamamatsu R3809U-50) is used as the detector (response time 40 ps). The instrument response function of the experimental set up is limited by the fwhm of the excitation laser pulse and is 75 ps for the 375 nm source. The lamp profile is recorded by scatterer (dilute Ludox solution in water) in place of the sample. Time-resolved fluorescence anisotropy decay profiles are analyzed by nonliner least-squares iteration procedures using F900 decay analysis software. The quality of the fit is accessed by the chi square (χ^2) values and distribution of residuals. Temperature is controlled by the Quantum Northwest (TC125) instrument. Time-resolved fluorescence anisotropy measurement is done using two polarizers by placing one of them in the excitation beam path and the other one in front of the detector. An alternate collection of the fluorescence intensity in parallel and perpendicular polarization (with respect to the vertically polarized excitation laser beam) for an equal interval of time has been carried out until the count difference between the two polarizations (at $t = 0$) is ~5000. For *G*-factor calculation, the same procedure is adopted but with 5 cycles and horizontal polarization of the exciting laser beam.

RESULT AND DISCUSSION

The time-resolved fluorescence anisotropy, r(t), is estimated using the following equation

$$r(t) = \frac{GI_{VV}(t) - I_{VH}(t)}{GI_{VV}(t) + 2I_{VH}(t)} \quad \text{where } G = \frac{\sum I_{HH}(t)}{\sum I_{HV}(t)} \qquad (1)$$

where G is the instrument correction factor for detector sensitivity to the polarization of the emission, which is 0.7 at the wavelength of detection. $I_{HH}(t)$ and $I_{HV}(t)$ are the intensity of fluorescence decays when the excitation and emission polarizers are polarized at horizontal−horizontal and horizontal−vertical alignment, respectively. Again, $I_{VV}(t)$ and $I_{VH}(t)$ are the intensity of fluorescence decays when the excitation and emission polarizers are polarized at vertical−vertical and vertical−horizontal alignment, respectively.

A. C-153. Representative anisotropy decay profiles of C-153 in the neat RTILs at various temperatures are shown in Figure 1. Figure 2, which shows the plot of ln(η) versus $1/T$ for the four ionic liquids, reveals that there is a gradual increase in the viscosity with an increase in the alkyl chain length on the sulfate anion. The rotational relaxation parameters for C-153 in the ILs at different temperatures are collected in Table 1. Both

dx.doi.org/10.1021/jp207528p |*J. Phys. Chem. B* 2012, 116, 194–202

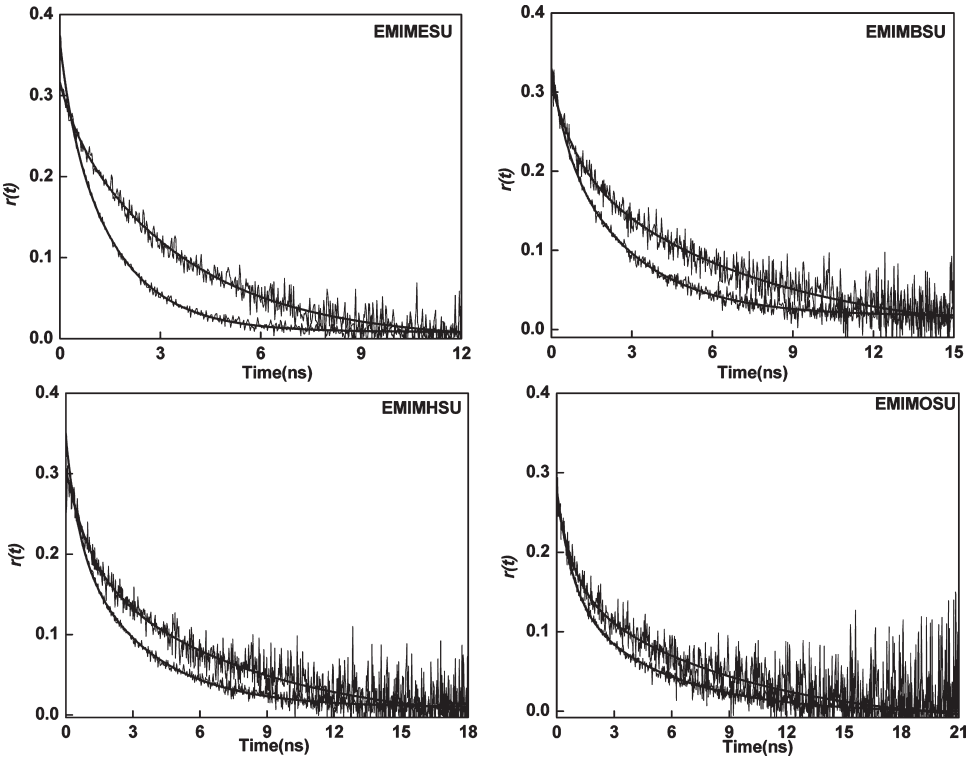

Figure 1. Anisotropy decay profiles of C-153 in four ionic liquids. Long and short decay profiles are at 293 and 313 K, respectively. Solid lines represent the biexponential fit to the data points.

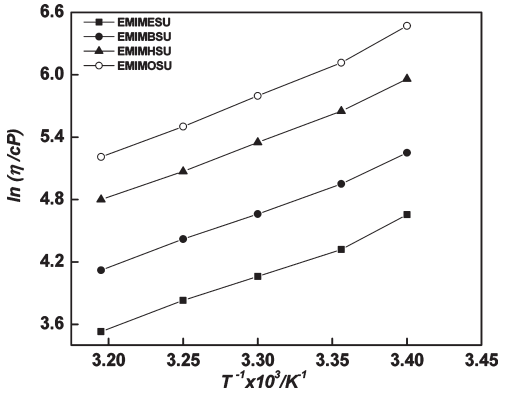

Figure 2. Plots of $\ln(\eta)$ versus $1/T$ for all four ILs. The line passing to the data points is drawn as a visual aid.

biexponential and single-exponential fits to the anisotropy decay profiles of C-153 in the ILs are acceptable. The biexponential fits are found to be slightly better than the single-exponential fits. However, the average rotational time, $\langle\tau_{rot}\rangle$, obtained from biexponential fits is found to be very similar to that obtained from single-exponential fits. The better fit of the anisotropy decay profiles using a biexponential decay function probably reflects the non-Markovian friction effects in these media. It may be mentioned in this context that Maroncelli and co-workers used a biexponential function to fit the anisotropy decays of C-153 in alcohols and other polar solvents, and have explained the observed behavior as a result of the non-Markovian nature of the friction.[43]

It is evident both from the anisotropy decay profiles shown in Figure 1 and the data presented in Table 1 that with an increase in temperature rotational diffusion becomes faster due to the lowering of the viscosity of the media. More interestingly, the data that are collected in Table 1 also reveal that the average rotational time of C-153 increases with an increase in the alkyl chain length of the ionic liquids. However, the decay does not become as slow as expected from the increase in the bulk viscosity values with a concomitant increase in the alkyl chain length. For example, at 293 K, on going from the ethyl to the butyl analogue, the average rotational time increases by 54% with a change in the viscosity value from 105 to 191 cP. However, on going from the butyl to the octyl analogue, the average rotational time changes by only 13% whereas the viscosity value changes by 455 units. This observation indicates that the rotational diffusion of C-153 actually becomes faster as we increase the alkyl chain length in the anionic moiety.

In an attempt to have a comprehensive understanding on the rotational dynamics of C-153, we analyzed our experimental data by the most commonly used Stokes−Einstein−Debye (SED) hydrodynamic model of rotational diffusion, according to which the rotational time (τ_r^{SED}) of noninteracting solute in a solvent continuum of viscosity η is given by

$$\tau_r^{SED} = \frac{V_h \eta}{k_B T} \quad (2)$$

where V_h is the hydrodynamic volume of the solute molecule and V_h is the product of the van der Waals volume V of the molecule, its shape factor f, and the boundary condition parameter C. T is

Table 1. Summary of the Rotational Relaxation Parameters of C-153 in RTILs at Different Temperatures

RTILs	temp (K)	bulk[a] viscosity (cP)	r_0[b]	a_1	τ_1 (ns)	a_2	τ_2 (ns)	$\langle\tau_{rot}\rangle$ (ns)[c]	C_{rot}[d]
EMIMESU	293	105	0.34	0.12	0.46	0.88	3.66	3.28	0.35
	298	75	0.36	0.19	0.90	0.81	3.34	2.88	0.43
	303	58	0.36	0.29	1.00	0.71	2.73	2.23	0.44
	308	46	0.33	0.21	0.71	0.79	2.10	1.81	0.46
	313	34	0.38	0.19	0.36	0.81	1.63	1.39	0.48
EMIMBSU	293	191	0.31	0.30	0.92	0.70	6.87	5.08	0.29
	298	141	0.34	0.29	0.77	0.71	5.16	3.88	0.31
	303	106	0.37	0.25	0.60	0.75	3.95	3.11	0.34
	308	82	0.36	0.30	0.66	0.70	3.30	2.51	0.35
	313	63	0.33	0.26	0.54	0.74	2.77	2.19	0.40
EMIMHSU	293	389	0.30	0.37	1.08	0.63	7.67	5.23	0.15
	298	284	0.31	0.34	0.89	0.66	5.77	4.11	0.16
	303	211	0.31	0.34	0.64	0.66	4.62	3.27	0.18
	308	160	0.30	0.35	0.67	0.65	4.20	2.96	0.21
	313	122	0.35	0.36	0.62	0.64	3.36	2.37	0.23
EMIMOSU	293	646	0.28	0.39	0.95	0.61	8.86	5.77	0.10
	298	453	0.28	0.42	0.93	0.58	7.28	4.61	0.11
	303	329	0.28	0.40	0.80	0.60	6.00	3.92	0.14
	308	245	0.28	0.41	0.75	0.59	5.51	3.56	0.17
	313	183	0.28	0.47	0.81	0.53	5.03	3.04	0.20

[a] ±5%. [b] Initial anisotropy. [c] Rotational relaxation time (error limit 5−10%). [d] Rotational coupling constant.

Table 2. Solute Dimensions and van der Waals Volumes Together with Shape Factors and Boundary Condition Parameters Calculated Using the SED Hydrodynamic Theory

solute	axial radii/Å^3	van der Waals volume/Å^3	shape factor (f)	boundary conditions (C_{slip})
C-153	6.0 × 3.9 × 2.5	243	1.5	0.18
AP	5.0 × 3.5 × 1.8	134	1.6	0.16

the absolute temperature, and k_B is the Boltzmann constant. The shape factor f depends on the axial ratio of the semi axes. For a spherical solute f is unity and greater than 1 for an asymmetric ellipsoid. When the size of the rotating solute is much bigger than the solvent molecule, the boundary condition parameter, C, is unity and represented as the stick boundary condition. In the case of a solute of comparable size, C is less than unity and remains commonly within the range $0 < C < 1$.

For calculation of the τ_r^{SED} values corresponding to the probes, we used the probe properties that are available in the literature.[23] The values for the probe molecules are collected in Table 2. Since all three axial radii are different, each solute molecule is treated as an asymmetric ellipsoid. The friction coefficients (ξ_i) with stick and slip boundary conditions along the three principle axes of rotation are estimated from the literature available numerical tabulations.[44,45] From the calculated friction coefficients, the diffusion coefficients along the three axes (D_i) are obtained using the following Einstein relation

$$D_i = \frac{k_B T}{\xi_i} \tag{3}$$

Considering that the direction of the transition dipole coincides with the long axis of the molecule, the rotational times are calculated from the diffusion coefficients by the following equation[46]

$$\tau_r = \frac{1}{12}\left(\frac{4D_a + D_b + D_c}{D_aD_b + D_bD_c + D_cD_a}\right) \tag{4}$$

where D_a, D_b, and D_c are the diffusion coefficients along the a, b, and c axes, respectively. The boundary condition (C_{slip}) is estimated from the calculated rotational times.

Figure 3 shows the log−log plots of the experimentally measured reorientation times of C-153 vs η/T in four ionic liquids along with the calculated stick and slip lines. As can be seen from Figure 3, the rotational dynamics of C-153 in EMIMESU lie between the stick and slip boundary conditions.

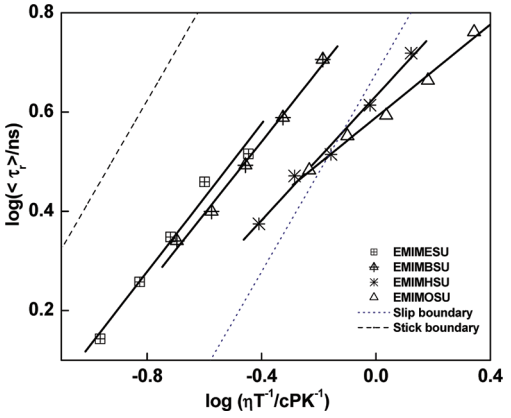

Figure 3. log−log plots of the average rotational relaxation time of C-153 vs η/T in different ILs with slip and stick boundary condition parameters. Symbols denote the experimental data points, and the solid line represents the linear fit to the data points.

dx.doi.org/10.1021/jp207528p | J. Phys. Chem. B 2012, 116, 194–202

Interestingly, Figure 3 also reveals that with an increase in the alkyl chain length on the sulfate moiety the rotational dynamics of C-153 changes to slip and finally reaches the subslip condition as in the case of the highest member (EMIMOSU) of the series. The faster rotation of C-153 with an increase in the alkyl chain length on the anionic constituent of the ILs is also evident when we fit the τ_r and η/T data for C-153 to the function $\tau_r = A(\eta/T)^p$, a procedure described by Mali et al.[29,30]

C-153 in EMIMESU

$$\tau_r = (7.042 \pm 0.76)(\eta/T)^{0.70 \pm 0.074} \quad (N = 5, R = 0.9857)$$

C-153 in EMIMBSU

$$\tau_r = (6.966 \pm 0.18)(\eta/T)^{0.76 \pm 0.029} \quad (N = 5, R = 0.998)$$

C-153 in EMIMHSU

$$\tau_r = (4.301 \pm 0.067)(\eta/T)^{0.64 \pm 0.037} \quad (N = 5, R = 0.9953)$$

C-153 in EMIMOSU

$$\tau_r = (3.871 \pm 0.063)(\eta/T)^{0.48 \pm 0.030} \quad (N = 5, R = 0.9944)$$

We also calculated the rotational coupling constant (C_{rot}) defined as $C_{rot} = \tau_{rot}/\tau_{stk}$, where τ_{rot} is the experimentally measured rotational time and τ_{stk}, is obtained with the help of eq 2. Interestingly, C_{rot} values (Table 1) indicate the faster rotation of C-153 with an increase in the alkyl chain length. It is pertinent to mention here that the study by Fruchey et al.[34] shows that the rotational behavior of perylene becomes increasingly subslip as the alkyl chain length on the cation moiety is increased. As mentioned earlier, no alkyl chain length dependence on the rotational dynamics of DMDPP in FAP-containing ILs has been observed.[31] In view of this, the rotational behavior of C-153 in different ionic liquids used in this work is quite interesting.

In this context, we note that the quasi-hydrodynamic theories of Gierer–Wirtz (GW)[47] and Dote–Kivelson–Schwartz (DKS)[48] tell that the size of the solvent molecules has a profound effect on solute rotation in the sense that larger solvent molecules provide lower friction to the rotating solutes. Consequently, boundary condition parameter C, obtained from SED theory, is modified by both GW and DKS theories. Since SED theory is not successful in explaining the rotational behavior of C-153 in the ILs (EMIMHSU and IMIMOSU), we resort to both the DKS[49−51] and the GW[43] models to explain the faster rotation of C-153 with increasing length of alkyl side chains.

According to GW theory, the solvent is made up of concentric shells of spherical particles surrounding the spherical solute molecule at the center. The boundary condition parameter (C_{GW}) is determined by considering the decrease in the angular velocity of the solvent molecules in successive shells surrounding the solute as a function of distance away from it. The boundary condition parameter is expressed by the following relation[47]

$$C_{GW} = \sigma C_0 \tag{5}$$

where σ is the sticking factor, which is given by the relation

$$\sigma = \left[1 + 6\left(\frac{V_S}{V_P}\right)^{1/3} C_0\right]^{-1} \tag{6}$$

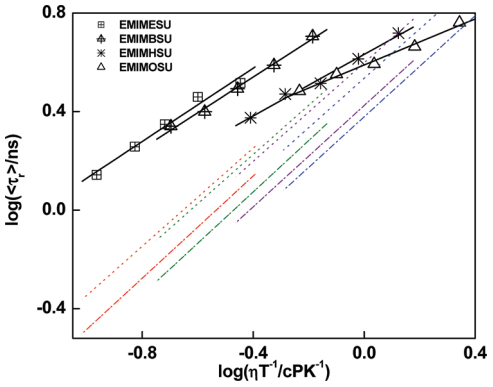

Figure 4. log–log plots of the average rotational relaxation time of C-153 vs η/T in different ILs with boundary condition parameters obtained from the DKS and GW models. Symbols denote the experimental data points, and the solid line represents the linear fit to the data points. Dotted and dash-dotted lines represent the boundary condition for the GW and DKS models, respectively (red = EMIMESU, green = EMIMBSU, purple = EMIMHSU, blue = EMIMOSU).

and C_0 is given by the following expression

$$C_0 = \left[\frac{6\left(\frac{V_S}{V_P}\right)^{1/3}}{\left[1 + 2\left(\frac{V_S}{V_P}\right)^{1/3}\right]^4} + \frac{1}{\left[1 + 4\left(\frac{V_S}{V_P}\right)^{1/3}\right]^3}\right]^{-1} \tag{7}$$

In the above relation V_S and V_P are van der Waals volume of the solvent and solute, respectively. The van der Waals volumes of the ILs are estimated using the Edward increment method.[52] Figure 4 depicts the log–log plots of the average rotational relaxation time of C-153 vs η/T in different ILs with boundary condition parameters obtained from the GW model. As can be seen from Figure 4, the GW model is quite successful in explaining the rotational dynamics of C-153 in EMIMHSU. However, in a larger system (EMIMOSU) the same model is found not to be so successful (Figure 4).

We also analyzed our data by employing the DKS model. DKS theory takes into account the free volume of the solvent along with the solvent to solute volume ratio while calculating the boundary condition parameter. The boundary condition parameter for the DKS model is given by the following relation[48]

$$C_{DKS} = (1 + \gamma/\varphi)^{-1} \tag{8}$$

where

$$\gamma = \frac{\Delta V}{V_P}\left[4\left(\frac{V_P}{V_S}\right)^{2/3} + 1\right] \tag{9}$$

and $\phi = fC_{slip}$, where C_{slip} is the solute–solvent coupling parameter under slip boundary condition.[53] In eq 9, ΔV is the smallest volume of free space per solvent molecule which is empirically related to the viscosity, Hilderbrand–Batschinski

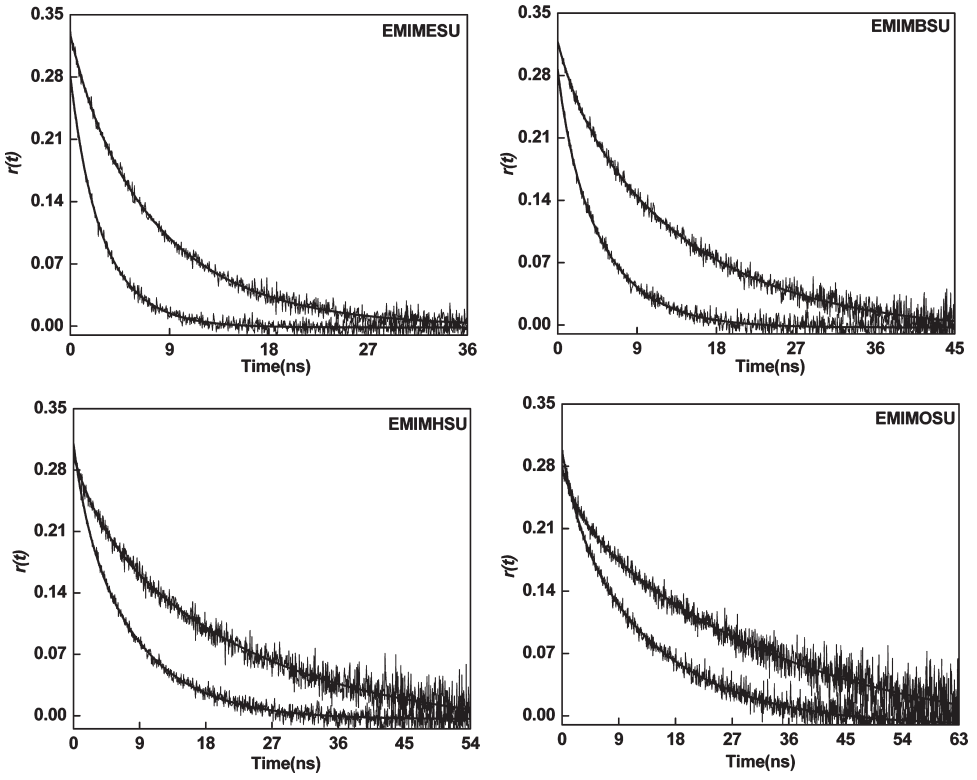

Figure 5. Anisotropy decay profiles of AP in the four ionic liquids. Long and short decay profiles are at 293 and 313 K, respectively. Solid lines represent the single-exponential fit to the data points.

Table 3. Summary of the Rotational Relaxation Parameters of AP in RTILs at Different Temperatures

system	temp (K)	bulk viscosity (cP)[a]	r_0[b]	$\langle\tau_{rot}\rangle$ (ns)[c]	C_{rot}[d]
EMIMESU	293	105	0.34	7.67	1.4
	298	75	0.36	5.84	1.5
	303	58	0.36	4.63	1.6
	308	46	0.33	3.76	1.6
	313	34	0.38	3.02	1.8
EMIMBSU	293	191	0.31	12.39	1.2
	298	141	0.34	9.63	1.3
	303	106	0.37	7.57	1.4
	308	82	0.36	6.00	1.4
	313	63	0.33	4.78	1.5
EMIMHSU	293	389	0.30	19.56	0.9
	298	284	0.31	15.80	1.1
	303	211	0.31	12.16	1.1
	308	160	0.30	9.26	1.1
	313	122	0.35	7.08	1.2
EMIMOSU	293	646	0.28	30.00	0.9
	298	453	0.28	23.28	1.0
	303	329	0.28	19.50	1.2
	308	245	0.28	15.60	1.3
	313	183	0.28	12.30	1.3

[a] ±5%. [b] Initial anisotropy. [c] Rotational relaxation time (error limit 5−10%). [d] Rotational coupling constant.

parameter, and isothermal compressibility of the solvent.[48] Anderton and Kauffman[50] have shown that in the case of

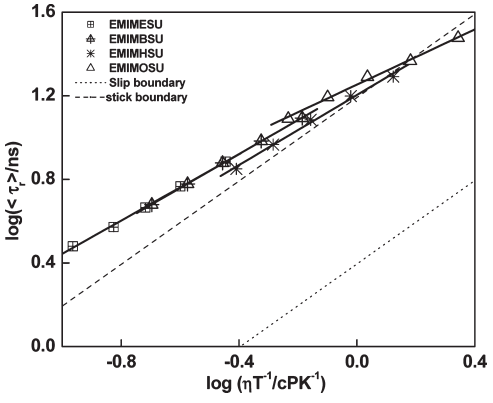

Figure 6. log−log plots of the average rotational relaxation time of AP vs η/T in different ILs with slip and stick boundary condition parameters. Symbols denote the experimental data points, and the solid line represents the linear fit to the data points.

associative solvents the measure of free volume can be represented by the following relation

$$\Delta V = V_m - V_s \quad (10)$$

where V_m is the solvent molar volume divided by the Avogadro number. Molar volumes of all the ILs have been calculated by estimating the density of the IL. There is a 4% decrease in the C_{DKS} values obtained for C-153/EMIMOSU solute−solvent combination from 293 to 313 K due to a decrease in the density of the media. Figure 4 depicts the log−log plots of the average rotational relaxation time of

dx.doi.org/10.1021/jp207528p |J. Phys. Chem. B 2012, 116, 194–202

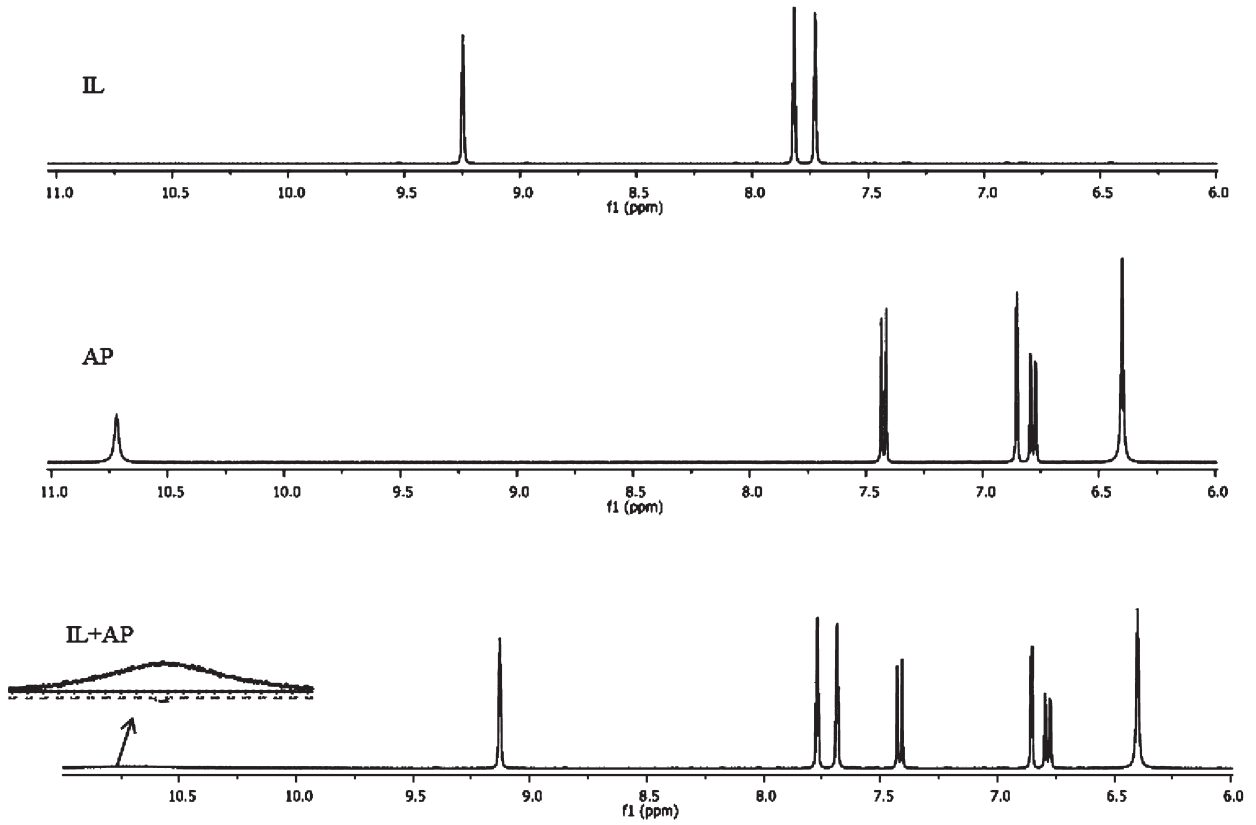

Figure 7. Proton NMR spectra for IL (EMIMESU), AP, and AP with IL in DMSO-d_6.

C-153 vs η/T in different ILs with boundary condition parameters obtained from the DKS model. The DKS model is successful in explaining the faster rotation of C-153 in EMIMOSU (Figure 4). The observation shows that the rotational behavior of C-153 is mainly governed by the size of the alkyl chains. Since the larger solvent molecules offer lower friction to the rotating solutes, the rotation of C-153 becomes faster with increasing length of alkyl side chains.

It may be mentioned in this context that the rotational dynamics in the subslip domain are sometimes attributed to the complex solvation structure near the probe molecule.[54,55] This structuring sometimes creates void spaces, which reduce the rotational friction below slip.

B. AP. Representative anisotropy decay profiles of AP in the neat RTILs at various temperatures are shown in Figure 5. We resort to single-exponential fitting for the anisotropy data of AP because a biexponential fit to the anisotropy data does not improve the quality of the fitting and also the average rotational time estimated from the biexponential fit is found to be very similar with that obtained from the single-exponential fit. The rotational relaxation parameters for AP in the ILs at different temperatures are collected in the Table 3.

As can be seen from Table 3, with an increase in temperature the rotational diffusion of AP becomes faster due to the lowering of the viscosity of the media. We also analyzed the rotational behavior of AP by the most commonly used Stokes–Einstein–Debye (SED) hydrodynamic model. In the case of AP, Figure 6 represents the log–log plots of experimentally measured reorientation times of AP vs η/T in four ionic liquids along with the calculated stick and slip lines. As can be seen from Figure 6, the rotational time of the AP is significantly higher than that predicted by the stick boundary condition in EMIMESU. This kind of behavior is known as "superstick" behavior, which indicates the strong association of the probe molecule with the solvent.[21] Here, we note that a recent study by Samanta and coworkers[35] shows that ethidium bromide (EB) follows superstick behavior in [bmim][BF_4] by virtue of solute–solvent hydrogen bonding. Again, Kurnikova et al.[56] also pointed the role of the hydrogen-bonding interaction in explaining the superstick behavior of thionine in dimethyl sulfoxide (DMSO). Hence, the present superstick behavior of the AP in the present ionic liquid can be attributed to the hydrogen-bonding interaction between AP and the ionic liquid. In this context, it is to be mentioned that the mere presence of a solute–solvent hydrogen bond may not slow down solute rotation. It should be strong enough such that the hydrogen-bonding dynamics takes place on a time scale that is comparable to or slower than solute rotational dynamics.[57] To confirm the hydrogen-bonding interaction, we also carried out a ^{1}H NMR investigation. A representative NMR spectrum showing the effect of solvent on the solute is shown in Figure 7. As can be seen, the N–H proton signal of AP which appears at 10.71 ppm becomes very broad in the presence of the IL. The present NMR results confirm the hydrogen-bonding interaction between the N–H fragment of AP and the sulfate moiety of the ionic liquid. Other ionic liquids also broaden the N–H proton signal. However, the extent of broadening is found to be so large that it has not been possible for us to differentiate the NMR line width with respect to the variation of chain length of ionic liquids. To find out the potential of AP as a H-bond donor, we carried the

charge density analysis by optimizing the structure of AP at the B3LYP[58,59]/6-31++G (d,p) level and using the Gaussian 03 program.[60] Considerable charge density on the hydrogen atoms of amine (0.290) and imide (0.320) indicate the acidic nature of the N−H hydrogens. Moreover, the ability of AP to act as a H-bond donor is also demonstrated by Dobek and co-workers.[61] They demonstrated that AP can form a hydrogen bond (N−H···O−S) with hydrogen-bond acceptors like dimethyl sulfoxide (DMSO) and sodium dodecyl sulfate (SDS). Quite interestingly, Figure 6 also reveals the influence of alkyl chain length on the rotational behavior of AP. Figure 6 clearly shows that the hydrodynamics of AP changes from superstick to stick with an increase in the alkyl chain length. The following relationship has been obtained when we fit the τ_r and η/T data for AP in to the function $\tau_r = A(\eta/T)^p$.

AP in EMIMESU

$$\tau_r = (17.392 \pm 0.324)(\eta/T)^{0.79 \pm 0.013} \quad (N = 5, R = 0.9996)$$

AP in EMIMBSU

$$\tau_r = (17.632 \pm 0.163)(\eta/T)^{0.81 \pm 0.011} \quad (N = 5, R = 0.9998)$$

AP in EMIMHSU

$$\tau_r = (15.795 \pm 0.244)(\eta/T)^{0.79 \pm 0.044} \quad (N = 5, R = 0.9960)$$

AP in EMIMOSU

$$\tau_r = (17.919 \pm 0.176)(\eta/T)^{0.65 \pm 0.017} \quad (N = 5, R = 0.9990)$$

We also measured the rotational coupling constants for AP in all four ILs (Table 3). At a particular temperature, C_{rot} values (Table 3) for AP are found to be considerably larger in the present ionic liquids than those[23] found in conventional non-hydrogen-bonding solvents. Since the rotational coupling constant (C_{rot}) represents the measure of the extent of departure from normal hydrodynamic behavior of a solute due to specific interaction, the present observation is a clear reflection of the hydrogen-bonding interaction between the AP and the ionic liquids. Upon careful observation we find that the value of C_{rot} decreases as we go from ethyl to hexyl and levels out at the octyl substituent. The average C_{rot} values are estimated to be 1.58, 1.36, 1.08, and 1.14 for the ethyl, butyl, hexyl, and octyl substituent, respectively (Table 3). To explain the present observation, we calculated the charge density on the oxygen atoms of the sulfate group by optimizing (at B3LYP/6-31++G (d,p) level) the structures of all four anions independently. The decrease in C_{rot} values with an increase in the alkyl chain length is in tune with the decrease in the total charge density [−2.766 (ethyl), −2.747(butyl), −2.727 (hexyl), and −2.729 (octyl)] on the four oxygen atoms of the sulfate group (H-bond acceptor) of alkyl sulfates. It has been reported in the case of substituted salicylates by Shan et al.[62] that the hydrogen-bond strength increases with an increase in the negative charge density on the hydrogen-bond acceptor. The present observation is interesting in a sense that the previous two literature reports, which depict the alkyl chain length dependence on the rotational dynamics of MPTS[34] and R110,[31] show that the values of rotational coupling constants increase with an increase in the alkyl chain length on the cationic moiety.

CONCLUSION

The rotational dynamics of two neutral organic solutes, coumarin-153 (C-153) and 4-aminophthalimide (AP), has been investigated in a series of 1-ethyl-3-methylimidazolium alkyl sulfate ionic liquids (alkyl = ethyl, butyl, hexyl, and octyl) with an aim to find out the effect of alkyl side chains on the rotational dynamics of the two organic solutes in these ionic liquids. The results obtained from the fluorescence anisotropy measurements indicate two distinct rotational environments for two different solutes. The rotational dynamics of C-153 lie between stick and slip boundary condition in the ethyl analogue and finally reaches the subslip condition as in case of the octyl substituent. The rotational dynamics of C-153 becomes faster with an increase in the alkyl chain length, primarily because of the fact that larger solvent molecules offer lower friction to the rotating solute. The hydrodynamic behavior of AP changes from superstick to stick with an increase in the alkyl chain length. Superstick behavior has been attributed to the strong solute−solvent hydrogen-bonding interaction between AP and the ionic liquid. Proton NMR results confirm a hydrogen-bonding interaction between the N−H hydrogen of AP and sulfate ion. Rotational coupling constant values have been found to decrease with increasing length of alkyl side chains. The observed rotational behavior of AP has been attributed to the decrease in the solute−solvent-specific interaction with an increase in the alkyl side chain length on the sulfate moiety.

AUTHOR INFORMATION

Corresponding Author
*Phone: +91-674-2304037. Fax: +91-674-2304050. E-mail: msarkar@niser.ac.in.

ACKNOWLEDGMENT

M.S. is thankful to the Department of Science and Technology (DST) for a generous research grant. The authors thank Dr. Bhaskar G. Dutt for stimulating discussion. Thanks are due to the Council of Scientific and Industrial Research (CSIR) for a fellowship to S.K.D.

REFERENCES

(1) Welton, T. *Chem. Rev.* **1999**, *99*, 2071.
(2) Wasserscheid, P.; Keim, W. *Angew. Chem., Int. Ed.* **2000**, *39*, 3772.
(3) Sheldon, R. *Chem. Commun.* **2001**, 2399.
(4) Dupont, J.; de Suza, R. F.; Suarez, P. A. Z. *Chem. Rev.* **2002**, *102*, 3667.
(5) Hayashi, S.; Ozawa, R.; Hamaguchi, H. *Chem. Lett.* **2004**, *33*, 1590.
(6) Chiappe, C.; Pieraccini, D. *J. Phys. Org. Chem.* **2005**, *18*, 275.
(7) Hough, W. L.; Rogers, R. D. *Bull. Chem. Soc. Jpn.* **2007**, *80*, 2262.
(8) Rogers, R. D.; Voth, G. A. *Acc. Chem. Res.* **2007**, *40*, 1077.
(9) Chiappe, C.; Konig, B.; Impareto, G. *Eur. J. Org. Chem.* **2007**, 1049.
(10) Rantwijk, F. V.; Sheldon, R. *Chem. Rev.* **2007**, *107*, 2757.
(11) Weingrätner, H. *Angew. Chem., Int. Ed.* **2008**, *47*, 654.
(12) Plechkova, N. V.; Seddon, K. R. *Chem. Soc. Rev.* **2008**, *37*, 123.
(13) Mandal, P. K.; Sarkar, M.; Samanta, A. *J. Phys. Chem. A* **2004**, *108*, 9048.
(14) Hu, Z.; Margulis, C. J. *Proc. Natl. Acad. Sci. U.S.A.* **2006**, *103*, 831.
(15) Wakai, C.; Oleinikova, A.; Ott, M.; Weingärtner, H. *J. Phys. Chem. B* **2005**, *109*, 17028.

(16) Stoppa, A.; Hunger, J.; Buchner, R.; Hefter, G.; Thoman, A.; Helm, H. *J. Phys. Chem. B* **2008**, *112*, 4854.
(17) Samanta, A. *J. Phys. Chem. B* **2006**, *110*, 13704.
(18) Adhikari, A.; Sahu, K.; Dey, S.; Ghosh, S.; Mandal, U.; Bhattacharyya, K. *J. Phys. Chem. B* **2007**, *111*, 12809.
(19) Samanta, A. *J. Phys. Chem. Lett.* **2010**, *1*, 1557.
(20) Paul, A.; Samanta, A. *J. Phys. Chem. B* **2007**, *111*, 4724.
(21) Ingram, J. A.; Moog, R. S.; Ito, N.; Biswas, R.; Maroncelli, M. *J. Phys. Chem. B* **2003**, *107*, 5926.
(22) Ito, N.; Arzhantsev, S.; Heitz, M.; Maroncelli, M. *J. Phys. Chem. B* **2004**, *108*, 5771.
(23) Ito, N.; Arzhantsev, S.; Maroncelli, M. *Chem. Phys. Lett.* **2004**, *396*, 83.
(24) Seth, D.; Sarkar, S.; Pramanik, R.; Ghatak, C.; Setua, P.; Sarkar, N. *J. Phys. Chem. B* **2009**, *113*, 6826.
(25) Sarkar, S.; Pramanik, R.; Ghatak, C.; Setua, P.; Sarkar, N. *J. Phys. Chem. B* **2010**, *114*, 2779.
(26) Castner, E. W., Jr.; Wishart, J. F.; Shirota, H. *Acc. Chem. Res.* **2007**, *40*, 1217.
(27) Funston, A. M.; Fadeeva, T. A.; Wishart, J. F.; Castner, E. W., Jr. *J. Phys. Chem. B* **2007**, *111*, 4963.
(28) Antony, J. H.; Mertens, D.; Dölle, A.; Wasserscheid, P.; Carper, W. R. *Chem. Phys. Chem.* **2003**, *4*, 588.
(29) Mali, K. S.; Dutt, G. B.; Mukherjee, T. *J. Chem. Phys.* **2005**, *123*, 174504.
(30) Mali, K. S.; Dutt, G. B.; Mukherjee, T. *J. Chem. Phys.* **2008**, *128*, 054504.
(31) Dutt, G. B. *J. Phys. Chem. B* **2010**, *114*, 8971.
(32) Dutt, G. B. *Ind. J. Chem.* **2010**, *49A*, 705.
(33) Karve, L.; Dutt, G. B. *J. Phys. Chem. B* **2011**, *115*, 725.
(34) Fruchey, K.; Fayer, M. D. *J. Phys. Chem. B* **2010**, *114*, 2840.
(35) Khara, D. C.; Samanta, A. *Phys. Chem. Chem. Phys.* **2010**, *12*, 7671.
(36) Santhosh, K.; Samanta, A. *J. Phys. Chem. B* **2010**, *114*, 9195.
(37) Santhosh, K.; Banerjee, S.; Rangaraj, N.; Samanta, A. *J. Phys. Chem. B* **2010**, *114*, 1967.
(38) Wu, H.; Wang, H.; Xue, L.; Shi, Y.; Li, X. *J. Phys. Chem. B* **2010**, *114*, 14420.
(39) Dutt, G. B. *ChemPhysChem* **2005**, *6*, 413.
(40) Chapman, C. F.; Fee, R. S.; Maroncelli, M. *J. Phys. Chem.* **1995**, *99*, 4811.
(41) Horng, M. L.; Gardecki, J. A.; Papazyan, A.; Maroncelli, M. *J. Phys. Chem.* **1995**, *99*, 17311.
(42) Das, S. K.; Sarkar, M. *Chem. Phys. Lett.* **2011**, *515*, 23.
(43) Horng, M.-L.; Gardecki, J. A.; Maroncelli, M. *J. Phys. Chem. A* **1997**, *101*, 1030.
(44) Small, E. W.; Isenberg, I. *Biopolymers* **1977**, *16*, 1907.
(45) Sension, R. J.; Hochstrasser, R. M. *J. Chem. Phys.* **1993**, *98*, 2490.
(46) Hartman, R. S.; Alavi, D. S.; Waldeck, D. H. *J. Phys. Chem.* **1991**, *95*, 7872.
(47) Gierer, A.; Wartz, K. *Z. Naturforsch. A* **1953**, *8*, 532.
(48) Dote, J. L.; Kivelson, D.; Schwart, R. N. *J. Phys. Chem.* **1981**, *85*, 2169.
(49) Roy, M.; Doraiswamy, S. *J. Chem. Phys.* **1993**, *98*, 3213.
(50) Anderton, R. M.; Kauffman, J. F. *J. Phys. Chem.* **1994**, *98*, 12117.
(51) Ben-Amotz, D.; Drake, J. M. *J. Chem. Phys.* **1988**, *89*, 1019.
(52) Edward, J. T. *J. Chem. Educ.* **1970**, *47*, 261.
(53) Hu, C. M.; Zwanzig, R. *J. Chem. Phys.* **1974**, *60*, 4354.
(54) Kim, Y. R.; Hochstrasser, R. M. *J. Phys. Chem.* **1992**, *96*, 9595.
(55) Mannekutla, J. R.; Ramamurthy, P.; Mulimani, B. G.; Inamder, S. R. *Chem. Phys.* **2007**, *340*, 149.
(56) Kurnikova, M. G.; Balabai, N.; Waldeck, D. H.; Coalson, R. D. *J. Am. Chem. Soc.* **1998**, *120*, 6121.
(57) Fleming, G. R. *Chemical Applications of Ultrafast Spectroscopy*; Oxford University Press: New York,1986.
(58) Becke, D. A. *J. Chem. Phys.* **1993**, *98*, 5648.
(59) Lee, C.; Yang, W.; Parr, R. G. *Phys. Rev. B* **1988**, *37*, 785.
(60) Frisch, M. J.; Trucks, G. W.; Schlegel, H. B.; Scuseria, G. E.; Robb, M. A.; Cheeseman, J. R.; Zakrzewski, V. G.; Montgomery, J. A., Jr.; Stratmann, R. E.; Burant, J. C.; Dapprich, S.; Millam, J. M.; Daniels, A. D.; Kudin, K. N.; Strain, M. C.; Farkas, O.; Tomasi, J.; Barone, V.; Cossi, M.; Cammi, R.; Mennucci, B.; Pomelli, C.; Adamo, C.; Clifford, S.; Ochterski, J.; Petersson, G. A.; Ayala, P. Y.; Cui, Q.; Morokuma, K.; Malick, D. K.; Rabuck, A. D.; Raghavachari, K.; Foresman, J. B.; Cioslowski, J.; Ortiz, J. V.; Stefanov, B. B.; Liu, G.; Liashenko, A.; Piskorz, P.; Komaromi, I.; Gomperts, R.; Martin, R. L.; Fox, D. J.; Keith, T.; Al Laham, M. A.; Peng, C. Y.; Nanayakkara, A.; Gonzalez, C.; Challacombe, M.; Gill, P. M.W.; Johnson, B.; Chen, W.; Wong, M. W.; Andres, J. L.; Gonzalez, C.; Head-Gordon, M.; Replogle, E. S.; Pople, J. A. *Gaussian 03*, Revision C.02; Gaussian, Inc.: Wallingford, CT, 2004.
(61) Maciejewski, A.; Kubicki, J.; Dobek, K. *J. Phys. Chem. B* **2003**, *107*, 13986.
(62) Shan, S.; Herschlag, D. *Proc. Natl. Acad. Sci. U.S.A.* **1996**, *93*, 14474.